Suppression of Ru (S = 1) spin dimerization in La2RuO5 by Ti substitution

S Riegg, Sebastian Widmann, A Günther, Hans-Albrecht Krug von Nidda, Armin Reller, Alois Loidl, Stefan G. Ebbinghaus

Angaben zur Veröffentlichung / Publication details:

Riegg, S, Sebastian Widmann, A Günther, Hans-Albrecht Krug von Nidda, Armin Reller, Alois Loidl, and Stefan G. Ebbinghaus. 2013. "Suppression of Ru (S = 1) spin dimerization in La2RuO5 by Ti substitution." *Journal of Physics: Condensed Matter* 25 (12): 126002. https://doi.org/10.1088/0953-8984/25/12/126002.

Suppression of Ru ($S = 1$) spin dimerization in La_2RuO_5 by Ti substitution

S Riegg[1], S Widmann[1], A Günther[1], H-A Krug von Nidda[1], A Reller[2], A Loidl[1] and S G Ebbinghaus[3]

[1] Experimental Physics V, Center for Electronic Correlations and Magnetism, University of Augsburg, D-86159 Augsburg, Germany
[2] Resource Strategy, University of Augsburg, D-86159 Augsburg, Germany
[3] Solid State Chemistry, Martin-Luther University Halle-Wittenberg, D-06099 Halle, Germany

E-mail: stefan.riegg@physik.uni-augsburg.de

Abstract

La_2RuO_5 shows a magneto-structural phase transition at 161 K with spin dimerization and concomitant formation of a non-magnetic singlet ground state. To gain a deeper insight into the origin of this transition systematic substitution of Ru by Ti has been carried out. Polycrystalline samples have been synthesized by thermal decomposition of citrate precursors leading to $La_2Ru_{1-y}Ti_yO_5$ ($0 \leq y \leq 0.45$). The crystal structure was investigated by x-ray powder diffraction at room temperature and at 100 K. The valences of Ti and Ru were obtained from x-ray absorption near edge structure spectroscopy at the Ti–K and the Ru–L_{III} absorption edges, respectively. The magnetic phase transition was investigated by magnetic susceptibility measurements as a function of Ti substitution, revealing a decreasing transition temperature on increasing the level of substitution. The step-like feature in the magnetic susceptibility reflecting the Ru–Ru spin dimerization transition becomes smeared out close to $y = 0.3$ and completely vanishes at $y = 0.45$, indicating complete suppression of spin-dimer formation. Additional specific-heat measurements show a continuous decrease of the magnetic entropy peak with increasing Ti substitution mirroring the reduced number of spin dimers due to the magnetic dilution. A magnetic anomaly of the dimerization transition can hardly be detected for $y \geq 0.3$. Density functional theory calculations were carried out to study changes of the electronic band structure caused by the substitution. A possibly preferred distribution of Ti and Ru and the magnetic interactions as well as the change of the density of states close to the Fermi level are investigated. Based on these experimental results a detailed (y, T) phase diagram is proposed.

1. Introduction

Perovskite related oxides containing ruthenium show a wide variety of interesting physical properties, e.g. different magnetic ordering phenomena, magnetic frustration, superconductivity or heavy-fermion behavior. These properties are often strongly influenced by the substitution of Ru by other metal cations. Titanium, for example, is a good candidate, since Ti^{4+} and Ru^{4+} possess a comparable ionic radius in octahedral coordination and Ti^{4+} is non-magnetic due to its $3d^0$ electronic ground state in contrast to the $4d^4$ ($S = 1$) electronic configuration of Ru^{4+}. As a result of the $3d^0$ configuration the +4 oxidation state is rather redox stable for Ti and therefore commonly found in oxide materials.

Titanium substitution was carried out previously for $SrRuO_3$ and the layered Sr_2RuO_4, for example, and typically leads to a metal to insulator transition and increased thermal stability of the compounds [1, 2]. Sr_2RuO_4 has been investigated extensively due to the occurrence of unconventional superconductivity at 0.93 K [3], which is suppressed by traces of Ti [2]. The ruthenates $LnCu_3Ru_4O_{12}$ (Ln = La, Pr, Nd) are heavy-fermion compounds, which show a change of various physical properties including a metal to insulator transition and the change from itinerant magnetism to local moments upon increasing Ti substitution [4–6].

La_2RuO_5 is another interesting ruthenate. It undergoes a phase transition at $T_d = 161$ K [7, 8], where the monoclinic high-temperature (ht-) crystal structure (space group $P2_1/c$, no. 14) changes to a triclinic low-temperature (lt-) modification (space group $P\bar{1}$, no. 2) within a temperature range of roughly 20 K for polycrystalline samples [9–11]. Simultaneously, the magnetic and electronic properties are modified and the ground state can be best described as a two-leg ladder of $S = 1$ spins with the rungs forming spin-singlets.

The ht-phase is a paramagnetic semiconductor with an activation energy of roughly 0.15 eV (determined from resistivity measurements) with localized $S = 1$ spin moments of the Ru^{4+} ions [7]. In figure 1 the crystal structure of the room-temperature structure is depicted. It can be described as an alternating stacking of LaO and $LaRuO_4$ layers along the a-axis. In the lt-modification the pairing of the $S = 1$ spin moments of the Ru^{4+} ions leads to a non-magnetic ground state and in turn a strongly suppressed magnetic susceptibility of roughly 10^{-4} emu mol^{-1}. This spin-Peierls-like dimerization into a singlet ground state results from small changes of interatomic distances and angles, i.e. alternating longer and shorter Ru–Ru distances and different Ru–O–Ru bond angles. The electronic band structures of the ht- and lt-modifications were modeled by density functional theory (DFT) calculations [12–14]. In the lt-phase the spin arrangement corresponds to a spin ladder in the bc-plane with antiferromagnetically arranged Ru–Ru dimers as rungs. In addition, an increased band gap in the lt-phase was calculated in accordance with the slightly increased conductivity activation energy of 0.21 eV [7]. The investigation of the specific heat of La_2RuO_5 and the comparison with different magnetic models like a 2D Heisenberg and a 3D spin-dimer system lead to the conclusion that the diminishing magnetic susceptibility in the lt-phase is caused by the formation of spatially isolated spin-singlets as a result of a structural phase transition [15].

The substitution of La by other rare-earth elements leading to $La_{2-x}Ln_xRuO_5$ (Ln = Pr, Nd, Sm, Gd, Dy) was described recently [5, 11]. The maximum substitution level was found to depend on the lanthanide ionic radii (the smaller the Ln^{3+} ion the lower the maximal x). For all substituted compounds the structural phase transition was observed, always occurring in combination with the Ru–Ru dimerization and concomitant spin-singlet formation [16]. This indicates that the structural changes caused by the substitution and additional magnetic moments of the rare-earth ions do not significantly influence the singlet ground state of the Ru spin system. We therefore tried to more directly affect the magnetic coupling by substituting Ru with Ti. Ti^{4+} is non-magnetic and, therefore, interrupts the magnetic exchange between the Ru $S = 1$ spins. Furthermore, Ti incorporation should affect the crystal structure because La_2TiO_5 crystallizes in an orthorhombic structure isostructural to Y_2TiO_5, which is completely different compared to the La_2RuO_5 structure [17–19].

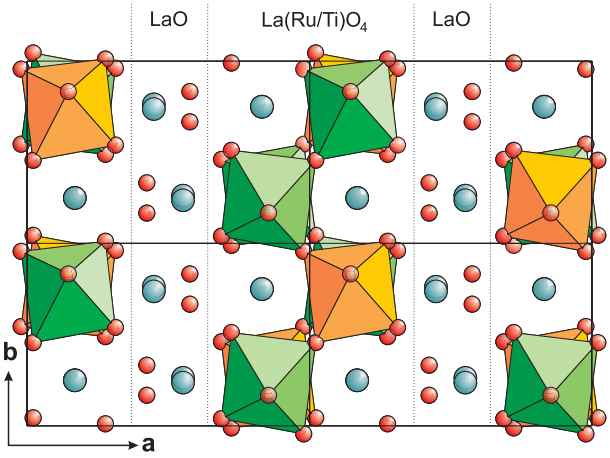

Figure 1. Crystal structure of $La_2Ru_{1-y}Ti_yO_5$ (2 × 2 unit cells) viewed along the c-axis. La is represented by turquoise spheres, oxygen by red spheres and RuO_6 octahedra are drawn in light green. The substitution of Ru by Ti is illustrated by orange TiO_6 octahedra. The alternating layering of LaO and $La(Ru/Ti)O_4$ is indicated along the a-axis.

We were not able to synthesize $La_2Ru_{1-y}Ti_yO_5$ samples by a conventional solid-state reaction. Thus, an adapted sol–gel route has been developed to obtain single phase samples up to $y = 0.45$. These were investigated in detail with respect to their crystal structure and the impact of emerging structural changes on the spin-Peierls-like transition. To deepen the understanding of the phase-transition behavior, the Ru and Ti oxidation states were determined by x-ray absorption near edge structure (XANES) spectroscopy. Furthermore, the entropy of the dimerization transition was investigated with specific-heat measurements to study the exchange interaction strength. In addition, DFT calculations were performed to support the interpretation of the experimental results of the magneto-structural transition.

2. Experimental details

2.1. Synthesis

For the soft-chemistry synthesis of polycrystalline $La_2Ru_{1-y}Ti_yO_5$ samples a precursor containing Ti was prepared according to the route described by Tada *et al* [20]. Two hundred milligrams of titanium metal powder (Aldrich, 99.7%) were dissolved in a mixture of 4 ml of 25% NH_3 (Merck) and 18.7 ml of 30% H_2O_2 (Merck, not H_3PO_4 stabilized) under water-bath cooling. The mixture was stirred until a clear yellowish solution was obtained and the Ti

powder was dissolved completely. By adding 3 moles of citric acid per mole of Ti an orange citratoperoxotitanate complex was stabilized. The excess H_2O_2 was decomposed by boiling the solution for roughly 1 h. Afterwards the solution was diluted with deionized water to 250 ml to obtain a precursor with a defined Ti concentration.

The preparation of the $La_2Ru_{1-y}Ti_yO_5$ samples started from an aqueous precursor solution (50 ml of deionized water) of $La(NO_3)_3 \times 6H_2O$ (Chempur, 99.9%) and ruthenium-nitrosyl acetate (Aldrich, 99.9%) in appropriate molar ratios to obtain 0.5 g of the final product. A small excess of roughly 2% of the lanthanum nitrate was required to obtain phase-pure products. The Ti precursor was added in corresponding amounts together with 3 moles of citric acid per mole of metal cation. The solutions were stirred and heated to 120 °C for roughly 4 h until gels formed. The gels were pre-reacted at 180 °C for 2 h and pyrolyzed at 600 °C for another 12 h. The resulting amorphous powders were well ground using an agate mortar and pestle and afterwards calcined in air in alumina crucibles for at least 96 h with intermediate grindings every 48 h. The phase purity was checked by x-ray powder diffraction after each of the grinding steps. The synthesis route is similar to the one described for rare-earth substituted $La_{2-x}Ln_xRuO_5$; however, for the Ti substitution water instead of ethanol was used as the solvent and a different Ru source was chosen [11].

2.2. Measurement techniques

Room-temperature x-ray powder diffraction (XRD) patterns were recorded in the angular range $10° \leq 2\theta \leq 150°$ using a Seifert 3003 TT powder diffractometer (Cu K$\alpha_{1,2}$ radiation). A one-dimensional single-line semiconductor detector (METEOR 1D) was used with a step width of 0.01° and an integration time of 300 s per data point. Additional low-temperature (100 K) and room-temperature XRD powder patterns were recorded using a STOE STADI P powder diffractometer with Cu Kα_1 radiation. The sample powders were diluted in a mass ratio of 1:3 with ground charcoal to reduce absorption and filled in capillaries of 0.3 mm diameter. A STOE IP-PDS detector (2θ range of 15°–130°) was used in combination with a flowing nitrogen cooling system (Oxford Cryosystems Cryostream 700). Ten patterns with an integration time of 600 s and a step width of 0.02°were accumulated for each sample for the Rietveld analysis [21].

Synchrotron x-ray diffraction patterns of polycrystalline $La_2Ru_{0.55}Ti_{0.45}O_5$ were recorded between 50 K and room temperature at the beamline B2 at HASYLAB, Hamburg [22]. The sample was mounted in a 0.3 mm diameter capillary. A wavelength of 0.562 85 Å (≈22 keV, Si-311 monochromator crystal) was used to measure the diffraction pattern in the angular range of $2° \leq 2\theta \leq 75°$ with steps of 0.008°. The data were recorded with the on-site readable image-plate detector OBI [23] with an integration time of roughly 15 min.

Crystal-structure analysis was carried out with the FULLPROF program suite [24]. The refinement of the La and O site occupancies leads to values very close to unity. In addition, the refinement of the Ru and Ti occupation factors leads to values very close to the nominal ones with deviations less than 1% (see supplementary information[4]).

Ru–L_{III} and Ti–K XANES measurements were carried out in transmission mode at the beamline A1 at HASYLAB. For the Ru–L_{III} edge measurements the sample powders were stuck to adhesive tape. The Ti–K edge measurements were performed utilizing pressed pellets (13 mm diameter) of a mixture of roughly 35 mg sample powder and 10 mg cellulose as a binder. All spectra were energy calibrated using Ru metal powder or Ti metal foil, respectively, as a reference.

Magnetic susceptibilities $\chi = M/H$ were investigated on a Quantum Design MPMS-XL superconducting quantum interference device (SQUID) magnetometer in the temperature range 2–400 K. Field cooled conditions with $H = 1000$ Oe are applied. The powder samples were enclosed in gel capsules whose small contribution to the measured magnetic susceptibility is taken into account by a temperature-independent fit parameter χ_0 in the data-fitting procedure.

The specific heat (C_p) at constant pressure was measured using a physical properties measurement system (PPMS) by Quantum Design in the temperature range between 1.8 and 300 K with a step width of 1 K. In the vicinity of the phase transition (±15 K) and below 30 K smaller temperature intervals of 0.2 K are used. Approximately 10 mg of sample powder and 2 mg of polyvinyl alcohol (PVA) were mixed, ground in an agate mortar and pressed into pellets of 3 mm diameter. The PVA contribution was subtracted from the recorded data. The fit of the lattice contribution was performed with the program Mathematica 7 applying an Einstein–Debye phonon model.

2.3. DFT calculation settings

The band structure calculations were performed using the full-potential local-orbital minimum base code implemented in the program FPLO 7.00-28 [25, 26]. The crystal-structure data obtained from XRD pattern refinement were used as input data. The symmetry was lowered to $P1$ (SG no. 1) to replace single Ru ions by Ti and to study the magnetic interaction of the Ru ions by using the local density approximation (LDA) and local spin density approximation (LSDA). The number of k points in the reciprocal lattice was adapted to the reciprocal unit-cell axis lengths and set to $3 \times 6 \times 4$. These values were chosen considering the limit of matrix elements available in the code settings used. A scalar relativistic setting was used for the calculations.

3. Results and discussion

The obtained black powder samples were investigated by XRD. Up to a substitution level of $y = 0.25$ no traces of impurities were detected, but for $y \geq 0.30$ an increasing

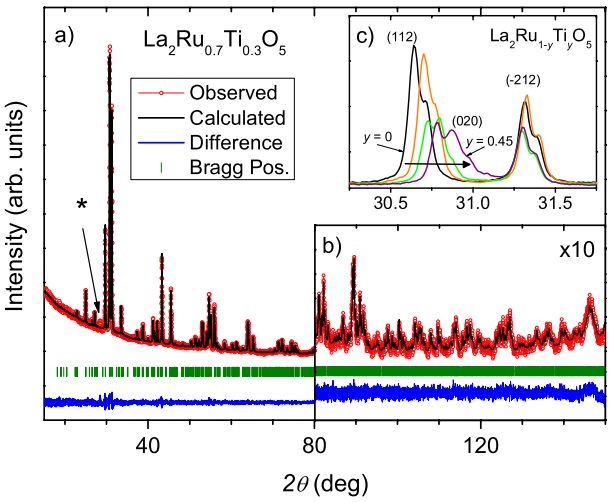

Figure 2. (a) Rietveld refinement of the $La_2Ru_{0.7}Ti_{0.3}O_5$ x-ray diffraction pattern, measured with Cu K$\alpha_{1,2}$ radiation at room temperature. The asterisk marks a trace of La_3RuO_7. For details see the text. The inset (b) shows a magnification (10×) of the angular range $80° \leq 2\theta \leq 150°$ to illustrate the good fit quality even at high diffraction angles. (c) Room temperature Cu K$\alpha_{1,2}$ x-ray diffraction patterns of La_2RuO_5 and Ti-substituted compounds with $y = 0.15, 0.30, 0.45$ in the region 30.25°–31.75° showing the evolution of selected Bragg-reflections (horizontal arrow) due to structural changes caused by the Ti substitution.

amount of La_3RuO_7 [27] up to roughly 1.5% ($y = 0.45$) was observed. This stems from the small excess of $La(NO_3)_3$, which is necessary to obtain single phase samples at lower substitution levels. The most intense reflection of the La_3RuO_7-pattern at roughly $2\theta = 28°$ is marked with an asterisk in figure 2(a). No additional peaks are observed, indicating that there is no long-range ordered superstructure of Ru and Ti and that the two elements are distributed statistically on the Ru/Ti sites.

The replacement of the Ru^{4+} ions (ionic radius 0.620 Å) by slightly smaller Ti^{4+} ions (0.605 Å) [28] in the octahedra of the $LaRuO_4$ layers causes structural stress and, therefore, only a partial substitution can be achieved. Although almost half of the Ru is substituted, no indications for the formation of the La_2TiO_5 structure are observed. For $y \geq 0.5$ the number of impurity phases increases dramatically. Therefore, these samples are not discussed in the following.

To investigate a possible influence of the synthesis method on the crystal structure and the physical properties, a batch of the unsubstituted La_2RuO_5 has also been synthesized by the above described soft-chemistry route. The obtained structural data are in good agreement with the previously reported samples synthesized by solid-state reaction, single-crystal growth and a different soft-chemistry approach [8, 9, 11, 29].

3.1. Crystal structure

The $La_2Ru_{1-y}Ti_yO_5$ powder samples crystallize in space group $P2_1/c$ in accordance with the unsubstituted La_2RuO_5. The Rietveld analysis of the XRD pattern of $La_2Ru_{0.7}Ti_{0.3}O_5$ recorded at room temperature is depicted in figures 2(a) and (b) as an example of the very good agreement of calculated pattern and measurement. Numerical values of the XRD Rietveld analysis results for all samples are listed in the supplementary information (see footnote 4) available at stacks.iop.org/JPhysCM/25/126002/mmedia.

In figure 2(c) the angular range $30.25° \leq 2\theta \leq 31.75°$ of the XRD patterns of pure La_2RuO_5 and selected Ti-substituted compounds with $y = 0.15, 0.30, 0.45$ are shown in more detail. The (0 2 0) peak is shifted with increasing y to higher 2θ values reflecting a shortening of the unit-cell parameter b. For the other two axes the influence of the substitution is much less pronounced. This observation is in clear contrast to the structural changes caused by rare-earth substitutions. In $La_{2-x}Ln_xRuO_5$ the a-axis is found to become particularly shorter, reflecting the incorporation of the smaller lanthanide ions in the LaO layers [11].

Numerical values for the room temperature unit-cell parameters obtained from the Rietveld refinements are depicted in figure 3(a) for a, b, and c and in figure 3(b) for β as a function of the substitution level y. The length of the a-axis slightly decreases up to $y = 0.25$ and then significantly increases. Upon substitution the b-axis decreases linearly by approximately 0.04 Å and, in contrast, the c-axis increases linearly with y. The most significant changes concern the b-axis (≈0.8%). Linked to the increase of c the monoclinic angle β (figure 3(b)) also increases linearly from approximately 100.75 to 101.2°. The behavior of β is similar to observations in $La_{2-x}Ln_xRuO_5$ with smaller rare-earth ions like Gd and Dy [11]. The limit of the structural changes is reached at ≈9.192 Å for a, at ≈5.79 Å for b and at ≈7.975 Å for c.

The changes of the unit-cell axes detected for the Ti-substituted samples are clearly different from those caused by rare-earth substitution, where all three axes were found to decrease with increasing substitution level [11]. This behavior is linked to the ionic radii of the smaller rare-earth ions compared to the La^{3+} ion. Consequently, the shrinkage of the cell parameters becomes stronger with decreasing ionic radius of Ln^{3+}. The rare-earth ions are preferably incorporated in the LaO layer [29]; therefore, in these compounds the a-axis shows the strongest decrease. Titanium, on the other hand, can only occupy the Ru site within the $LaRuO_4$ layers. As described above, this affects the Ru–O distances, as reflected by the b- and c-axis variation. The a-axis which is related to the interlayer distance is therefore rather undistorted.

The relative changes of the unit-cell parameters are shown in figure 3(c). The values were calculated by normalizing the cell parameters of the substituted samples to the corresponding cell parameters of La_2RuO_5. A linear behavior is observed for all cell parameters except for a and the unit-cell volume. They show a significant kink at $y \approx 0.25$. β, c, and a increase by roughly 0.4, 0.2 and 0.1%, respectively. In contrast, b decreases strongly by approximately 0.75%, in turn causing a decrease in the unit-cell volume. The anomalies detected close to $y \approx 0.25$ could indicate that for $y \geq 0.3$ no structurally long-range ordered dimerized ground state can be established. Despite these clearly observable changes, it is

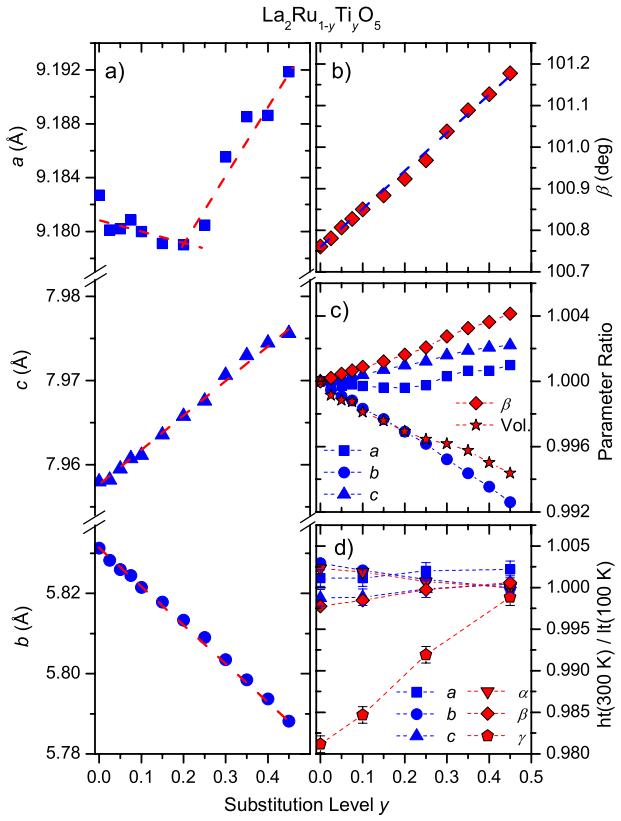

Figure 3. Cell parameters for $La_2Ru_{1-y}Ti_yO_5$ derived from Rietveld analysis of powder XRD data at room temperature. (a) Cell parameters a, b and c. (b) Monoclinic angle β. Error bars are less than the size of the symbols. (c) Relative change of the cell parameters. The cell parameters of $La_2Ru_{1-y}Ti_yO_5$ were divided by their corresponding values for La_2RuO_5. (d) Comparison of the cell parameters for the high-temperature (300 K) and low-temperature phases (100 K) of $La_2Ru_{1-y}Ti_yO_5$. Values of α and γ are 90° in the ht-phase.

noteworthy that the maximum relative change is below 1%, which is not surprising considering the small difference of the ionic radii of Ru^{4+} and Ti^{4+}.

In previous investigations we have studied the ruthenium–oxygen distances of La_2RuO_5 by powder neutron diffraction and single-crystal XRD [9, 29]. The Ru–O distances range between 1.933 and 2.067 Å. The shorter Ru–O bonds (O3, O4) are pointing to the LaO layers, while the longer bonds (O2 and O5) are cross-linking the corner-sharing octahedra in the $LaRuO_4$ layer. For $La_2Ru_{1-y}Ti_yO_5$ similar values are obtained, i.e. the shape of the octahedra is barely influenced by the substitution and the observed changes in the unit-cell parameters b and c are correlated to the angles between the octahedra. Although the Rietveld analysis of x-ray diffraction measurements yields structural information on the oxygen atoms with a somewhat broader error range than neutron diffraction data, the accuracy is sufficient to monitor the evolution of the corresponding bond angles with Ti substitution. It is found that the O5–Ru–O5 and the O2–Ru–O2 angles in the octahedra remain almost constant with values of approximately 95° and 178°, respectively, which is in good agreement with neutron diffraction results for La_2RuO_5 [9]. Furthermore, the Ru–O2–Ru angle along the c-axis of $La_2Ru_{1-y}Ti_yO_5$ is similar (153(1)°) to that of La_2RuO_5 (152.5°). In contrast, the value for Ru–O5–Ru increases significantly from 155.4° for La_2RuO_5 to roughly 160° with increasing Ti substitution level y. This results in a reduced tilting of the octahedra in the ab-plane, which causes the observed decrease in the unit-cell parameter b and also explains the slightly increasing values of a at higher substitution levels.

Bond-valence sum (BVS) calculations based on the XRD data were performed, from which the formal valences of the ions were derived [30]. In the $LaRuO_4$ layers of the Ti-substituted compounds valences of +3.0 for La, −2.0 for O and +4.0 for Ru are found in perfect agreement with the formal charges. The slightly smaller ionic radius of Ti compared to Ru results in a smaller value for the oxidation state of roughly +3.9. In the LaO layers deviations of the valences due to the shortened La–O distances are observed. Oxidation states of approximately +3.3 and −2.5 for La and O, respectively, are obtained. This effect has already been described for unsubstituted La_2RuO_5 and corresponds to smaller La sites and larger O sites in the LaO layers compared to the $LaRuO_4$ layers [11].

The evolution of the unit-cell parameters in the lt-phases of selected $La_2Ru_{1-y}Ti_yO_5$ compounds was investigated by XRD at 100 K. Samples with $y = 0, 0.1, 0.25$ and 0.45 were used for the measurements. For better comparability the room-temperature cell parameter data were divided by their corresponding values obtained at 100 K. The results are shown in figure 3(d). For unsubstituted La_2RuO_5 γ increases distinctly by approximately 1.8% due to the phase transition, while all other cell parameters remain basically constant (changes below 0.3%). These findings are in good agreement with previous investigations [9, 11]. From figure 3(d) it can be seen that the ratios of ht- and lt-parameters approach unity with increasing level of titanium substitution. This indicates that the structural phase transition is progressively suppressed by the incorporation of Ti. A comparison of the synchrotron radiation ($\lambda = 0.562\,85$ Å) XRD patterns of $La_2Ru_{0.55}Ti_{0.45}O_5$ at 50 and 300 K shows no significant difference, implying that the structural transition is completely suppressed for this substitution level. The results from magnetic measurements discussed in the following clearly support this finding of the absence of a structural transition for $y = 0.45$.

In addition, the thermal contraction of the unit-cell volume for $La_2Ru_{0.55}Ti_{0.45}O_5$ from room temperature down to 50 K has been determined. The thermal expansion coefficient $\alpha_c = 24.2(2) \times 10^{-6}$ K^{-1} derived from the fit according to $V = V_{300\,K} \exp(-\alpha_c \Delta T)$ is in the usual range for inorganic oxide materials [31]. Below 100 K the contraction and, thus, α_c decreases, which is a commonly observed behavior since the thermally activated vibration of the ions in solids freezes with decreasing temperature [32].

3.2. Valence determination using XANES

To investigate the influence of the substitution on the oxidation state of Ru and Ti, XANES measurements of the

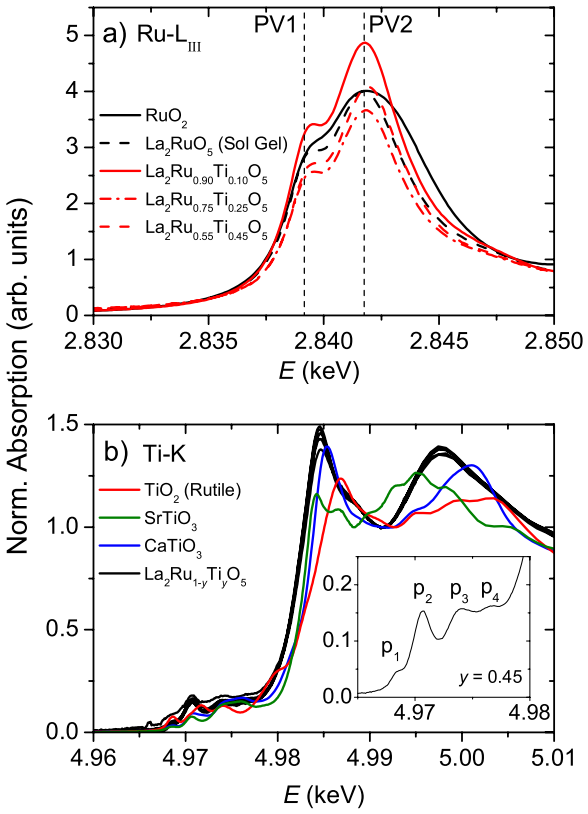

Figure 4. (a) Normalized Ru–L_{III} absorption spectra of RuO_2, La_2RuO_5 and $La_2Ru_{1-y}Ti_yO_5$ samples. The dashed vertical lines mark the positions of the two pseudo-Voigt fit maxima of a La_2RuO_5 reference sample prepared by solid-state reaction. (b) Normalized Ti–K absorption spectra of TiO_2, (Ca, Sr)TiO_3 and $La_2Ru_{1-y}Ti_yO_5$. The inset shows the characteristic pre-edge region of $La_2Ru_{0.55}Ti_{0.45}O_5$.

Ru–L_{III} (2.838 keV) and Ti–K (4.966 keV) absorption edges were performed [33].

In figure 4(a) the normalized Ru–L_{III} XANES spectra of selected samples ($La_2Ru_{0.9}Ti_{0.1}O_5$, $La_2Ru_{0.75}Ti_{0.25}O_5$ and $La_2Ru_{0.55}Ti_{0.45}O_5$) and references ($La_2RuO_5$ and RuO_2) are depicted. The intense white lines at roughly 2.84 keV resulting from $2p \rightarrow 4d$ excitations were modeled using two pseudo-Voigt (PV) functions to account for the octahedrally split 4d e_g and t_{2g} levels and an arctangent function, which is assigned to the edge jump of the absorption [34]. The least squares fit was performed with the program WinXAS [35]. The obtained positions of the two pseudo-Voigt peaks are taken for determining the oxidation state. By comparing these values with those of the reference materials, the valence of the ions can be determined since the edge energies are shifted to higher values by roughly 1–2 eV per integer step in oxidation state, which is known as the valence shift. La_2RuO_5 and RuO_2 are used as Ru^{4+} reference materials [29, 34, 36]. The energy positions of the two peaks are shown in comparison in the right frame of figure 5. From the almost identical values for the samples and references an oxidation state of Ru^{4+} for all samples can be deduced.

The ratio of the pseudo-Voigt peak areas (PV2/PV1) decreases from 6.57 ($y = 0, 0.10$) to 5.16 for $y = 0.45$. This can be explained by energetically closer 4d e_g states (d_{z^2} and $d_{x^2-y^2}$) and, therefore, points to a less distorted octahedral symmetry than described for $La_{2-x}Sr_xCu_{1-y}Ru_yO_{4-\delta}$ for example [34]. The crystal structures obtained from XRD and neutron powder diffraction are in agreement with this explanation. Furthermore, the constant distance of approximately 2.6 eV between the PV-peak maxima is in good agreement with the value found for tetravalent Ru [34].

The normalized spectra of the Ti–K edge measurements are depicted in figure 4(b). Reference materials are TiO_2 and the perovskite compounds (Ca, Sr, Eu)TiO_3, in which titanium is tetravalent. The spectra of all $La_2Ru_{1-y}Ti_yO_5$ samples are very similar, which reflects a constant Ti valence and oxygen coordination in the TiO_6 octahedra. In addition, the BVS calculations reveal almost constant Ti–O distances for all substitution levels y, which is also in agreement with this finding. The first maximum of the derivatives of the spectra is taken as the edge energy. In the left panel of figure 5 the energies of the tetravalent references and the samples are depicted. All $La_2Ru_{1-y}Ti_yO_5$ samples possess the oxidation state +4 within the error bars, as expected.

The inset of figure 4(b) shows the pre-edge region of the Ti–K absorption edge of $La_2Ru_{0.55}Ti_{0.45}O_5$. Four separate peaks ($p_1$–$p_4$) can be distinguished, which belong to the quadrupolar and dipolar transitions from the 1s to the higher 3d and 4p states [37]. In addition, the spectra are very similar to the Ti pre-edge region found for $BaTiO_3$, which is known for off-center positions of Ti in the octahedra at room temperature [37]. This observation is in agreement with the deviating Ru/Ti–O distances within the octahedra derived from the Rietveld refinements. The pre-edge feature shapes are almost identical for all titanium contents indicating that the metal–oxygen coordination remains basically identical for all $La_2Ru_{1-y}Ti_yO_5$ samples. It would be very interesting to check if the Ti off-center positions result in a polar ground state of Ti-substituted La_2RuO_5.

3.3. Magnetic properties

The unsubstituted La_2RuO_5 shows a paramagnetic behavior above the phase transition. In the low-temperature modification the measured magnetic susceptibility χ drastically decreases to a low value of roughly 10^{-4} emu mol^{-1} due to the Ru–Ru spin-singlet formation, which is described as a spin-Peierls-like transition [12, 14, 15]. Due to their $3d^0$ electronic configuration, the Ti^{4+}-ions have no paramagnetic moment. A substitution of Ru^{4+} ($S = 1$) by Ti^{4+} ($S = 0$) is expected to strongly influence the magnetic properties of $La_2Ru_{1-y}Ti_yO_5$ according to an increasing dilution of the Ru–Ru magnetic exchange and a concomitant suppression of the dimerization.

In figure 6 the magnetic susceptibilities of selected $La_2Ru_{1-y}Ti_yO_5$ samples with steps of $y = 0.05$ are depicted. For clarity the curves are shifted by a constant value. The increase of χ at very low temperatures is caused by remaining unpaired Ru^{4+} spin moments showing a paramagnetic behavior. They amount to approximately 1% for pure La_2RuO_5 [15] and increase slightly to a few

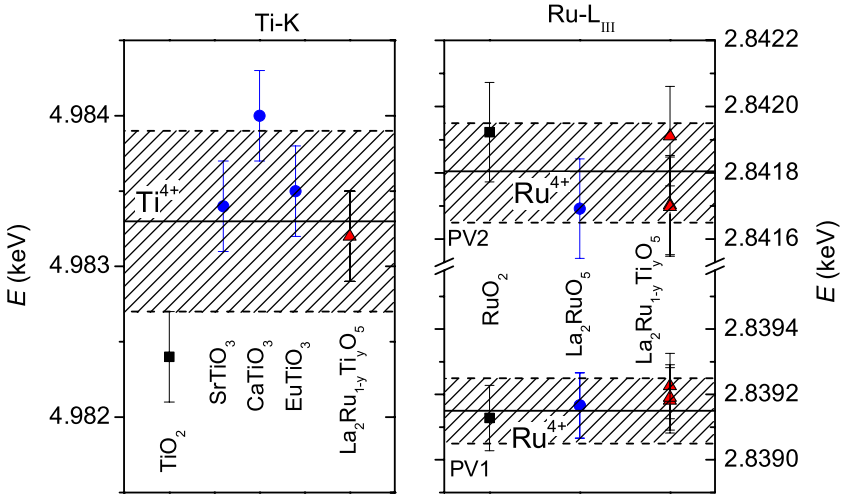

Figure 5. Left: Ti valence determined from the maxima of the first derivatives of the Ti–K XANES spectra. Right: Ru valence determined from the fit of the first derivative of the Ru–L_{III} XANES, the symbols represent the pseudo-Voigt maxima. Shaded energy intervals indicate the average Ti^{4+} and Ru^{4+} energies determined from the reference compounds. Dashed horizontal lines mark the estimated error window.

per cent with increasing Ti substitution level. Obviously, the magnetic transition temperature is strongly shifted (as indicated by the dashed line) and the reduction of χ below the transition temperature becomes less pronounced with increasing substitution level. In addition, the transition becomes broader. For $y \geq 0.3$ the step in χ becomes increasingly smeared out and for $y \geq 0.45$ the step has completely vanished, indicating that the Ti substitution locally inhibits the Ru–Ru dimerization. This is the first hint that a long-range dimerized ground state cannot be established for $y \geq 0.3$ and becomes completely suppressed for $y > 0.4$. This simply is a consequence of the statistical dilution of Ru dimers in the zig zag chains of the $LaRuO_4$ layers and the decreasing magnitude of the structural transition with increasing y.

By fitting $1/\chi$ above 200 K with a modified Curie–Weiss law $\chi = C/(T - \Theta_{CW}) + \chi_0$ the effective magnetic moment n_{eff} and the Curie–Weiss temperature Θ_{CW} in this paramagnetic range were calculated. A temperature-independent correction term χ_0 in a typical range of 10^{-4} emu mol^{-1} was added to account for possible van Vleck and diamagnetic contributions. The obtained values for n_{eff} are depicted in figure 7(a) in units of Bohr magneton μ_B. A decrease of the magnetic moment with increasing Ti substitution level is observed, in agreement with the dilution caused by non-magnetic Ti^{4+} ions.

The theoretical effective magnetic moments of the $La_2Ru_{1-y}Ti_yO_5$ samples were calculated using the spin-only value for Ru^{4+} and the Ru-substitution $(1-y)$ according to the equation $n_{eff} = \sqrt{(1-y)}n_{eff,Ru^{4+}}$. The corresponding result is drawn as a solid red line in figure 7(a). A value of 2.89 μ_B was obtained for the unsubstituted La_2RuO_5 indicating the Ru^{4+} magnetic moment $n_{eff,Ru^{4+}}$. It corresponds well to the theoretical spin-only value of 2.83 μ_B for $S = 1$. A good agreement of calculated and fit values for n_{eff} is observed in figure 7(a), therefore the model of non-magnetic Ti ions diluting the paramagnetic Ru^{4+} centers provides an appropriate description for the ht-phase of $La_2Ru_{1-y}Ti_yO_5$.

The Curie–Weiss temperatures Θ_{CW} obtained from the fit are depicted in figure 7(b). Starting from $\Theta_{CW} \approx$

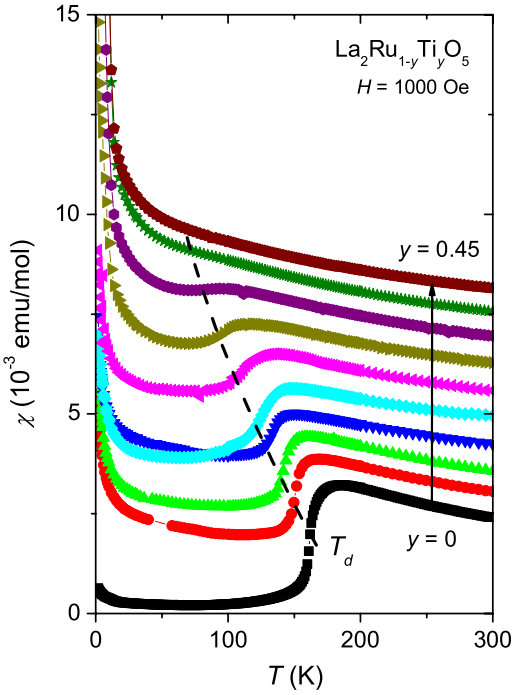

Figure 6. Magnetic susceptibilities of selected $La_2Ru_{1-y}Ti_yO_5$ samples with steps of $y = 0.05$ increasing from bottom to top (indicated by the vertical arrow). The χ curves are shifted by a constant value for clarity. The dashed line indicates the change of T_d with increasing substitution level.

-160 K for La_2RuO_5, it increases to roughly -105 K for $La_2Ru_{0.55}Ti_{0.45}O_5$ reflecting a successive reduction of the antiferromagnetic exchange in the paramagnetic phase. This effect again is caused by the dilution with the non-magnetic Ti^{4+} ions and is assumed to lead to a behavior indicated by the dashed red line, which is drawn to guide the eye. However, an unexpected minimum is observed at roughly $y = 0.2$ ($La_2Ru_{0.8}Ti_{0.2}O_5$) at which Θ_{CW} reaches approximately -185 K. At the same substitution level the step in the magnetic susceptibility changes from a sharp to

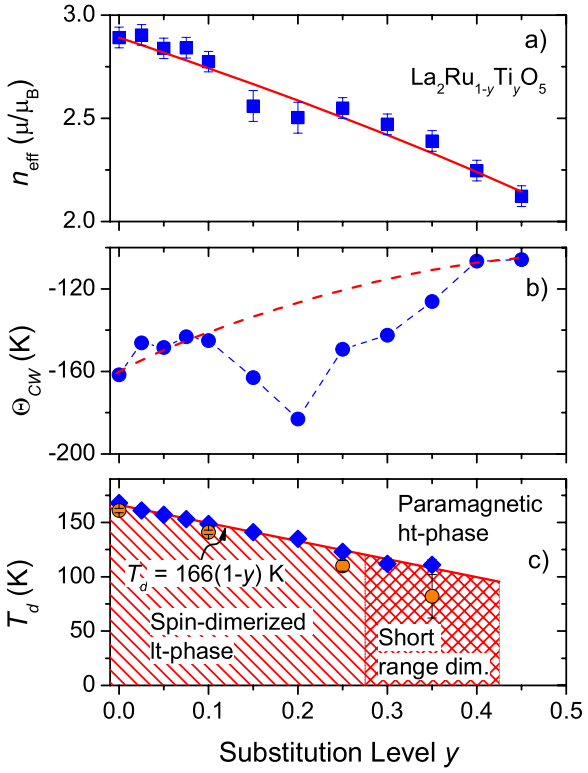

Figure 7. Effective magnetic moments n_{eff} (a) and Curie–Weiss temperatures Θ_{CW} (b) of $La_2Ru_{1-y}Ti_yO_5$ determined from the high-temperature range fit of $1/\chi$. The solid line in (a) marks the theoretical values for n_{eff} and the dashed line in (b) represents the assumed evolution for Θ_{CW}. For details see the text. (c) Transition temperatures of $La_2Ru_{1-y}Ti_yO_5$ obtained from magnetic susceptibility data. The solid red line is a linear fit between $y = 0$ and $y = 0.25$ (continued to $y = 0.425$), which reflects Vegard's law in agreement with the changes in the crystal structure caused by the substitution with smaller Ti^{4+} ions. The shaded red area marks the region of the spin dimerized phase for $y \leq 0.25$ and a short-range dimerized phase for $y \geq 0.3$ (cross shaded). Orange circles represent the peak-maxima temperatures from specific-heat data described in section 3.4.

a smoother and broader shape (figure 6) and n_{eff} shows a local minimum (figure 7(a)). The occurring minima can possibly be explained by two antagonistic effects, namely the increasing antiferromagnetic exchange interaction due to the decreasing interatomic distances in the crystal structure and the dilution caused by the diamagnetic Ti^{4+}. For small substitution levels the first effect apparently dominates. However, above $y = 0.2$ the effect of dilution becomes stronger than the increase of (nearest-neighbor) antiferromagnetic exchange and, hence, a rapid increase of Θ_{CW} is observed (figure 7(b)). More interestingly this behavior correlates with the starting significant increase of the cell parameter a at low doping levels up to $y = 0.2$ (figure 3(a)), which can be ascribed to the emerging changes in the crystal structure caused by the Ti substitution. This once more corroborates the close relationship between crystal structure and physical properties.

The dimerization temperature T_{d} corresponding to the transition from the ht- to the lt-phase was obtained from the inverse susceptibility according to the procedure described in [11]. In figure 7(c) T_{d} is depicted as blue diamonds versus the Ti concentration. The transition temperature reveals a linear decrease, which can be fit by $T_{\mathrm{d}} = 166(1 - y)$ K (solid red line in figure 7(c)). Above a substitution level of 0.25 the determination of T_{d} becomes increasingly uncertain due to the decreasing step height in $1/\chi$. For this reason the values for $y = 0.3$ and 0.35 are omitted in the fit. The corresponding area of the spin dimerized phase below T_{d} is shaded red for $y < 0.3$ to descriptively separate the paramagnetic and the dimerized phases in the diagram. Furthermore, a cross-shaded area representing short-range ordered clusters of Ru–Ru dimers is shown for $0.3 \leq y \leq 0.425$. T_{d} decreases linearly, and thus would become zero for a complete substitution of Ru by Ti and the subsequent structural changes according to Vegard's law. Due to the dilution the cooperative structural distortion is weakened and, hence, the intradimer exchange decreases.

Taking into account the observed linear T_{d} decrease and the vanishing of the transition step for $y = 0.45$ the absence of the structural transition also needs to be discussed in this context. The Rietveld analysis of the diffraction pattern recorded at 100 K leads to similar cell parameters and almost equal fit quality regardless of the starting model (i.e. the monoclinic ht- or the triclinic lt-structure). Most prominently, the ratio of γ is changing from $\approx$0.982 for $y = 0$ to roughly unity for $y = 0.45$, as shown in figure 3(d). Even in the high resolution synchrotron data no structural changes are detectable down to 50 K. Thus, $La_2Ru_{0.55}Ti_{0.45}O_5$ does not undergo a structural phase transition in agreement with the magnetic susceptibility data (figure 7(c)). This finding indicates that the spin-Peierls transition is actually driven by structural changes at T_{d} in the $La_2Ru_{1-y}Ti_yO_5$ compounds. Without additional energetic stabilization of the Ru orbitals by the structural modifications the resulting increased Ru–O–Ru superexchange and, hence, the spin dimerization cannot be observed [15, 16].

3.4. Specific heat

To deepen the understanding of the relationship between magnetic and structural phase transitions, the specific heat of selected samples was measured. In figure 8(a) C_p/T for La_2RuO_5, $La_2Ru_{0.9}Ti_{0.1}O_5$, $La_2Ru_{0.75}Ti_{0.25}O_5$, $La_2Ru_{0.65}Ti_{0.35}O_5$ and $La_2Ru_{0.55}Ti_{0.45}O_5$ is depicted. To increase the comparability the curves are shifted by 0.125 J mol^{-1} K^{-2}. All samples show similar phononic contributions, but with significant differences at the phase transition. The shape of the peak changes with increasing substitution level. A broadening from La_2RuO_5 to $La_2Ru_{0.75}Ti_{0.25}O_5$ is observed; however, the peak is less asymmetrically broadened than is found for rare-earth substituted samples [16]. The observed broadening may be caused by local inhomogeneities of the Ti substitution, minor impurities (La_3RuO_7) and different crystallinity of the samples due to varying calcination times. With increasing Ti substitution level the peak successively diminishes and cannot be clearly detected for $y \geq 0.35$. At lower substitution levels the transition temperature of the onset point of the high-temperature side of the peak complies well with the temperature derived from the magnetic susceptibility measurements described above (figure 7(c)).

Table 1. Results of the heat capacity fit for $La_2Ru_{1-y}Ti_yO_5$ (see text for details). The excess entropy contribution S^*_{mag} is calculated from the integrated residual peak after the subtraction of the lattice contribution and is normalized to the Ru content.

Sample	Θ_D (K)	Θ_{E1} (K)	Θ_{E2} (K)	Θ_{E3} (K)	Θ_{E4} (K)	S^*_{mag} (J mol^{-1} K^{-1})
La_2RuO_5 [16]	132	175	217	325	520	4.2(3)
$La_2Ru_{0.9}Ti_{0.1}O_5$	131	182	231	351	552	4.0(3)
$La_2Ru_{0.75}Ti_{0.25}O_5$	134	176	219	328	542	4.4(3)

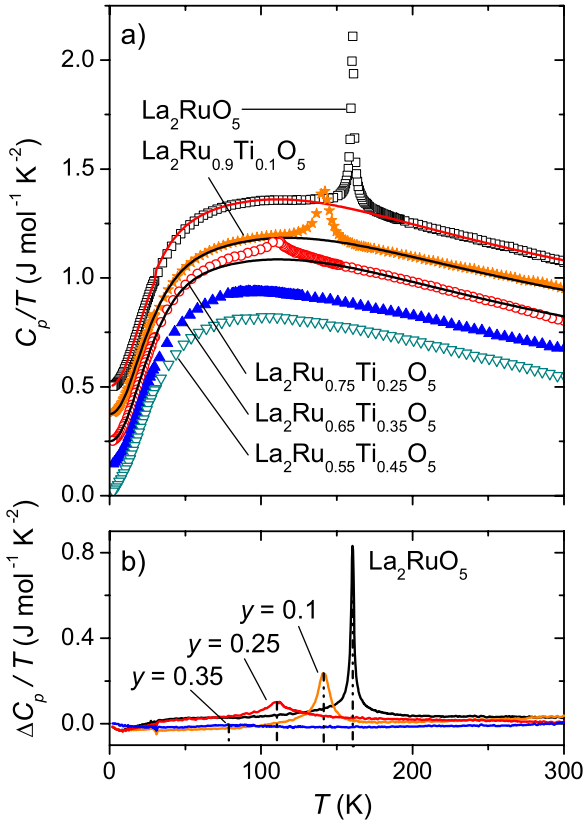

Figure 8. (a) Temperature dependence of the specific heat in representation C_p/T versus T of La_2RuO_5 and selected $La_2Ru_{1-y}Ti_yO_5$ samples (symbols). For clarity the curves are shifted by 0.125 J mol^{-1} K^{-2}. The solid lines mark the Einstein–Debye fits (see text). (b) Excess specific heat $\Delta C_p/T$ after subtraction of the $La_2Ru_{0.55}Ti_{0.45}O_5$ heat capacity curve. The vertical dash dotted lines mark the values of T_d shown in figure 7(c).

The lattice contributions for samples up to $y = 0.25$ were fitted using an Einstein–Debye phonon model. The eight terms of the fit, one for each atom per independent crystallographic site, are weighted according to the following scheme: $1 \times \Theta_D$:$1 \times \Theta_{E1}$:$1 \times \Theta_{E2}$:$1 \times \Theta_{E3}$:$4 \times \Theta_{E4}$. This scheme, which reduces the number of fit parameters to five, is derived from the low symmetrical crystal structure containing independent La, Ru and O sites. Only the four oxygens constituting the RuO_6 octahedra are combined to one term and, therefore, are weighted fourfold. Θ_D and Θ_{E1} to Θ_{E4} correspond to Debye and Einstein terms with their characteristic temperatures. In table 1 the calculated values for the Debye- and Einstein-temperatures are listed. These temperatures are very similar for all investigated compounds and they correspond well to values obtained for the rare-earth substituted compounds [16]. To improve the quality of the fit, a small constant offset value of approximately 2.3(2) mJ mol^{-1} K^{-2} is added. This small contribution to the specific heat, which is linear in T, would be due to free charge carriers, but in the doped samples rather stem from local disorder resulting in a linear glass-like contribution. The calculated parameters are in agreement with previously reported specific-heat data of La_2RuO_5 and, thus, indicate a semiconducting behavior for all Ti substitution levels [10, 16].

To obtain the magnetic entropy S_{mag} the Einstein–Debye fit curves were subtracted from the experimental data. The remaining residual peak was integrated between approximately 50 and 250 K according to $S_{mag} = \int C_p/T\,dT$. To simplify the interpretation of the values for S_{mag}, they were normalized with respect to the substitution level (i.e. divided by $1 - y$) and listed as S^*_{mag} in table 1. The entropy of pure La_2RuO_5 is expected to be $\Delta S = R\ln(3) - 0.5S_{dimer}$ according to [15, 16]. S_{dimer} is the entropy obtained for a single spin dimer and is weighed by 0.5, since the number of dimers is only half that of single spins. Due to the increasing incorporation of Ti the number of dimers decreases, because each single Ti impedes the formation of one spin dimer. The prefactor 0.5 should therefore decrease due to the lower number of remaining dimers. In [15, 16] a description of S_{mag} depending on J_0/k_BT_d has been introduced, where J_0 represents the exchange interaction strength within the dimers. Since the entropy values of the three samples are very similar, the intradimer exchange decreases with higher Ti incorporation according to the lower transition temperatures T_d.

In an alternative, more straightforward analysis the heat capacity of $La_2Ru_{0.55}Ti_{0.45}O_5$ was subtracted from the experimental data for the other samples. The residual curves are depicted in figure 8(b). While for the samples with low Ti substitution the transition peak is clearly observable, for $La_2Ru_{0.65}Ti_{0.35}O_5$ the peak is severely smeared out and almost undetectable. This could be explained by the absence of a true structural phase transition and that for $y \geq 0.3$ only short-range dimerization occurs with local clusters of Ru–Ru dimers which would not lead to a sharp peak in C_p. The transition temperatures determined from the peak maxima are shown as orange circles in figure 7(c). They agree fairly well with the above described transition temperatures of the dimerization transition.

The results of the XRD investigations, the magnetic and the C_p measurements clearly prove the close correlation between structural and physical features in Ti-substituted La_2RuO_5. With increasing Ti content the structural changes occurring at the phase transition become gradually smaller and for $y = 0.45$ they cannot be detected at all (figure 3(d)). Simultaneously, the step-like decrease in the magnetic

susceptibility diminishes and also the peak in C_p is suppressed. Already for $y = 0.3$ it is difficult to identify a sharp step at all. The variation of χ and C_p can be understood by a dilution of the interacting Ru moments by the non-magnetic Ti ions. This dilution reduces the number of remaining Ru spin dimers by the statistical distribution of Ru and Ti on the same crystallographic sites. Therefore, the reduced interaction only allows the formation of local dimers for $y > 0.25$. Also, it has to be noted that the formation of spin-singlets is closely linked to the crystallographic phase transition, which results in alternating short and long Ru–Ru distances within the RuO_4 zig zag chains. At the critical level of $y \approx 0.3$ the Ru–Ru interaction therefore becomes too small and/or the strain due the incorporated Ti ions becomes too large to allow the crystallographic transformation and, hence, the formation of spin dimers is impeded more strongly than those derived from only the Ru/Ti distribution and becomes completely suppressed for $y = 0.45$.

3.5. Band structure calculation

Calculations of the electronic band structures of Ti-substituted La_2RuO_5 were performed as described in [16] using the crystal structures determined by x-ray powder diffraction as input data. Due to the reduction of the symmetry into space group $P1$ it is possible to study the changes in the DOS and the electronic band structure when one or two Ru ions are replaced by Ti. This replacement corresponds to the compositions $La_2Ru_{0.75}Ti_{0.25}O_5$ and $La_2Ru_{0.5}Ti_{0.5}O_5$, respectively. The crystal structure of the latter was calculated by a linear extrapolation of the cell parameters and by using the atomic coordinates of the sample with the highest available substitution level $y = 0.45$. Several configurations of Ru and Ti on the four sites in the crystal structure were modeled and in addition the signs of the initial magnetic moments changed for different spin-polarized calculations to investigate their possible influences on calculated antiferromagnetic and ferromagnetic interactions.

In figure 9 the obtained DOS for the ht-modifications of La_2RuO_5 (c), $La_2Ru_{0.75}Ti_{0.25}O_5$ (b) and $La_2Ru_{0.5}Ti_{0.5}O_5$ (a) are shown. In the modeling of the ht-phase LDA has been used, because of the absence of magnetic ordering. The overall DOS and the partial DOS (pDOS) of Ru (red) and Ti (green) are shown in the range between -8 and 3.5 eV with respect to the Fermi level (E_F). The results for La_2RuO_5 (figure 9(c)) are in very good agreement with data published earlier [12, 14].

The overall DOS structure of La_2RuO_5 can be divided into three main parts [12, 13]. Starting approximately 1 eV above E_F the contribution of the 4d e_g levels of Ru are dominant, at roughly 3.5–4 eV the empty La 4f levels are located. Around E_F the Ru 4d t_{2g} and the O 2p levels belonging to the RuO_6 octahedra can be identified. From roughly -1.5 to -7 eV a large number of bands is present reflected by the large observed DOS in this range. This energy region can further be divided in two main regions. Between -1.5 and -4 eV the contributions from the O 2p levels of the LaO and $LaRuO_4$ layers are found. The range -4 to -8 eV can be assigned to the Ru 4d and O 2p of the $LaRuO_4$ layers.

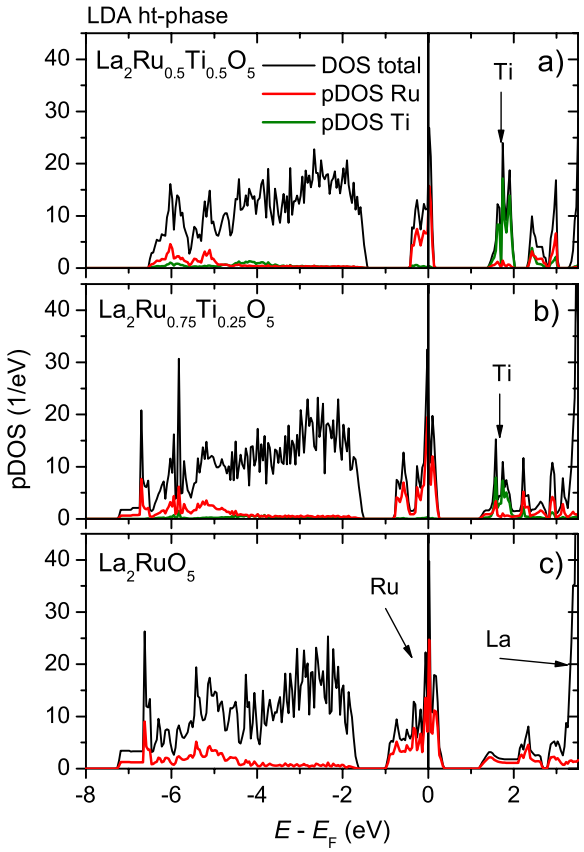

Figure 9. Comparison of the density of states of (a) $La_2Ru_{0.5}Ti_{0.5}O_5$, (b) $La_2Ru_{0.75}Ti_{0.25}O_5$ and (c) La_2RuO_5 using the LDA.

The DOS related to the LaO layers is barely influenced by the Ti substitution due to comparably small changes of the interatomic distances and coordinations. The charge of the corresponding oxygen is found to be higher than -2 for the three compounds, in agreement with the BVS calculations described above and results published earlier [16]. The charges of the other ions are roughly in agreement with their respective values from the BVS calculation as well.

With increasing Ti substitution, changes are observed, especially in the range above the Fermi energy by the appearance of unoccupied Ti 3d levels between 1 and 2 eV. In addition, the Ru contributions at E_F and below -4 eV are considerably smaller consistent with the decreasing Ru amount in the compounds. The energy range of the Ru 4d orbitals near E_F is significantly reduced from 1.5 eV for La_2RuO_5 to 0.8 eV for $y = 0.5$ reflecting the increasing localization of the Ru moments. This effect is in contrast to the broadening of the Ru bands observed for rare-earth substitutions, where this broadening has been used to explain the lowering of T_d due to the delocalization of the Ru spin moments [11, 16, 38]. In the present $La_2Ru_{1-y}Ti_yO_5$ samples the strongly reduced value of T_d merely reflects the decreasing number of Ru–Ru spin-singlets as a result of the suppressed structural transition. Furthermore, it can be seen that the distance between the centers of the Ru e_g and t_{2g} bands amounts to approximately 2.5 eV, identical for all three Ti substitution levels. This finding is in good agreement with the Ru–L_{III} XANES fit results, where also a constant energy

difference of 2.6 eV between the two pseudo-Voigt peaks at the absorption edge is determined (figure 4(a)), which can be ascribed to excitations into the 4d e_g and t_{2g} states.

In space group $P1$ there are four possible Ru sites per unit cell, on which the Ti atoms can be placed for the modeling. A comparison of the four possibilities of replacing one Ru atom by Ti in $La_2Ru_{0.75}Ti_{0.25}O_5$ was executed. All LDA calculations of the ht-phase lead to almost identical results in total energy and DOS, which shows that Ti can statistically occupy any one of the Ru sites. Since all possible arrangements lead to identical energy values no long-range cationic ordering and in turn no crystallographic superstructure is expected, which is in agreement with the XRD results. Similar investigations were performed for the ht-phase of $La_2Ru_{0.5}Ti_{0.5}O_5$; however, in this case a slightly (by less than 0.1 eV) preferred Ti distribution was found. The most stable result with lowest total energy is a checkerboard-like distribution of Ru and Ti ions, i.e. all Ru ions are surrounded by Ti and vice versa. This also is not found by XRD, but very probably exists on a local scale.

In addition, a number of different types of calculations using LDA and LSDA were carried out for the modeling of the lt-modification of $La_2Ru_{0.75}Ti_{0.25}O_5$. The LDA results of the ht- and lt-phase are similar and the deviations are caused by slightly different crystal structures (figure 3(d)) corresponding to the effects observed for unsubstituted La_2RuO_5 [12, 14, 16]. The similarity to the dimerized lt-phase of pure La_2RuO_5 has been checked for $La_2Ru_{0.75}Ti_{0.25}O_5$ by LSDA modeling. A preference of roughly 0.3 eV in total energy is found for an antiferromagnetic setting. The local spin moments of Ru amount to $S_\uparrow \approx 1.3$ and $S_\downarrow \approx 1.2$ and result in a total magnetic moment of $\pm 2\ \mu_B$ per formula unit (f.u.) with respect to the initial random orientation of the Ru spin moments. The result of the preserved ordering in the lt-phase is in excellent agreement with the above described results from magnetic and specific-heat measurements.

For $La_2Ru_{0.5}Ti_{0.5}O_5$ identical crystal structures were applied for the ht- and lt-modification according to the XRD results discussed above. Different LSDA scenarios were tested. It was found that the total energies only slightly favor the LDA results and all different sets of the Ru/Ti distribution representing the magnetic nearest-neighbor interactions lead to similar results. Using the preferred checkerboard distribution, the resulting Ru spin moments amount to $S \approx 1.4$ and a total magnetization of $+4\ \mu_B$/ f.u. is obtained for the ferromagnetic arrangement. Thus, for $y = 0.5$ (respectively 0.45) the ferromagnetic next-nearest-neighbor interactions seem to dominate the antiferromagnetic nearest-neighbor interactions when the checkerboard arrangement is present.

The DFT calculation results strongly support the above described findings of the dimerized state of lt-$La_2Ru_{0.75}Ti_{0.25}O_5$ and the absence of spin-singlets in $La_2Ru_{0.5}Ti_{0.5}O_5$.

4. Summary and conclusions

The synthesis of partially substituted $La_2Ru_{1-y}Ti_yO_5$ was carried out successfully up to a substitution level $y = 0.45$ by using a soft-chemistry route based on the thermal decomposition of a citrate based precursor. The Rietveld analysis of powder XRD data recorded at room temperature and 100 K reveals that the a-axis slightly increases only for $y > 0.2$, whereas the length of the b-axis decreases continuously. The c-axis as well as the monoclinic angle β increase linearly with increasing substitution level. The rotation of the RuO_6 octahedra causes higher Ru–O–Ru angles in the ab-plane, while the angle in the c-direction increases only slightly. A decreasing absolute change between the ht- and the lt-structures is observed with higher Ti contents. For $y = 0.45$ the structural phase transition is completely suppressed.

XANES measurements at the Ru–L_{III} and Ti–K absorption edges reveal oxidation states of +4 for both Ti and Ru for all samples. A detailed study of the white line at the Ru–L_{III} edge and the pre-edge region of the Ti–K edge indicates very similar (distorted) octahedral oxygen coordinations for all samples up to $y = 0.45$, in agreement with the results of the XRD investigations.

With increasing substitution level a distinct change of the magnetic susceptibility is observed. The strong suppression of χ below the phase-transition temperature, described as a spin-Peierls-like transition for La_2RuO_5, becomes less pronounced with increasing y and finally vanishes for $y > 0.4$. The magnetic moments derived from a Curie–Weiss fit of $1/\chi$ are in agreement with the sum of the remaining Ru^{4+} moments. The absolute values of the negative Θ_{CW} decrease with increasing y; however, a minimum for $y = 0.2$ is observed, which indicates increasing antiferromagnetic exchange due to the shorter interatomic distances. At higher substitution levels the Ru dilution is starting to dominate the magnetic exchange and the absolute value of Θ_{CW} decreases. The transition temperatures obtained from $1/\chi$ decrease linearly with higher substitution level.

A phase transition is clearly observable in the specific heat up to $y = 0.25$. With increasing substitution level this peak becomes broader, most likely because of local inhomogeneities in the Ti concentration. After subtraction of the lattice contribution using an Einstein–Debye phonon fit, the magnetic entropy is obtained from an integration between approximately 50 and 250 K. The peak area decreases with increasing y, reflecting a smaller number of Ru spin dimers, and the decreasing intradimer exchange J_0 correlates with the decreasing transition temperature. No transition can be observed for $y > 0.3$ due to the breakdown of the antiferromagnetic nearest-neighbor interaction. This results in the suppression of the long-range ordered singlet ground state, yielding only isolated spin-dimer clusters on a local scale. XRD, magnetic and C_p measurements show the close correlation between structural and physical properties. Both the structural phase transition and the changes in χ and C_p are successively reduced with increasing Ti content and completely suppressed for $y = 0.45$.

The comparison of DFT calculations for $La_2Ru_{0.75}Ti_{0.25}O_5$ and $La_2Ru_{0.5}Ti_{0.5}O_5$ with unsubstituted La_2RuO_5 show the location of the Ti states at roughly 1.5 eV above E_F and in turn a decrease of the Ru-pDOS at E_F. Spin-polarized

calculations for the lt-phase of $La_2Ru_{0.75}Ti_{0.25}O_5$ reveal that the antiferromagnetic arrangement known from lt-La_2RuO_5 is preserved, despite the incorporated non-magnetic Ti ions. This finding is in agreement with the specific heat and susceptibility results, both indicating the transition to a long-range dimerized state. For $y = 0.5$ (LSDA) the weak ferromagnetic exchange interactions of Ru–Ru next-nearest neighbors seem to be stronger than the antiferromagnetic exchange leading to the dimerization, which is in agreement with the absence of the singlet state for this substitution level.

The successful substitution of Ru^{4+} ions by non-magnetic Ti^{4+} is a very useful method to study the relationship between crystal structure and physical properties. Since Ru^{4+} and Ti^{4+} ions are almost equal in size, the magnetic properties are strongly influenced while only minor structural changes occur. Ti impedes both the spin dimerization and the structural phase transition. Increasing the Ti concentration leads to a breakdown of the long-range ordered spin-singlet formation and the transformation into a low-temperature structure with local Ru–Ru spin-singlets for $0.3 \leq y < 0.45$. The changes in the magnetic susceptibility and the heat capacity can be well explained by the dilution of Ru centers with increasing Ti content and in turn the reduced number of Ru spin dimers. The coupled breakdown of the spin dimerization for $y \geq 0.45$ can be reasoned because of its connection with the structural changes between room-temperature and low-temperature phases, which follow exactly the same trend, i.e. they become smaller with increasing Ti content and diminish for $y = 0.45$. It remains to be clarified if these structural changes are driven by the magnetic exchange interactions.

Acknowledgments

The authors gratefully acknowledge Dana Vieweg for SQUID and low-temperature XRD measurements. Additional thanks are due to HASYLAB for allocating beamtime and E Welter (A1) and A Bell (B2) for their kind technical support. This work was supported by the Deutsche Forschungsgemeinschaft within the collaborative research unit TRR 80 (Augsburg, Munich).

References

[1] Oswald H R, Felder-Cassagrande S and Reller A 1993 *Solid State Ion.* **63–65** 565–9
[2] Pucher K *et al* 2002 *Phys. Rev.* B **65** 104523
[3] Maeno Y, Hashimoto H, Yoshida K, Nishizaki S, Fujita T, Bednorz J G and Lichtenberg F 1994 *Nature* **372** 532–4
[4] Ramirez A P, Lawes G, Li D and Subramanian M A 2004 *Solid State Commun.* **131** 251–5
[5] Ebbinghaus S G, Riegg S, Götzfried T and Reller A 2010 *Eur. Phys. J. Spec. Top.* **180** 91–116
[6] Büttgen N, Krug von Nidda H-A, Kraetschmer W, Günther A, Widmann S, Riegg S, Krimmel A and Loidl A 2010 *J. Low Temp. Phys.* **161** 148–66
[7] Khalifah P, Osborn R, Huang Q, Zandbergen H W, Jin R, Liu Y, Mandrus D and Cava R J 2002 *Science* **297** 2237–40
[8] Boullay P, Mercurio D, Bencan A, Meden A, Drazic G and Kosec M 2003 *J. Solid State Chem.* **170** 294–302
[9] Ebbinghaus S G 2005 *Acta Crystallogr.* C **61** i96–8
[10] Malik S K, Kundaliya D C and Kale R D 2005 *Solid State Commun.* **135** 166–9
[11] Riegg S, Sazama U, Fröba M, Reller A and Ebbinghaus S G 2011 *Phys. Rev.* B **84** 014403
[12] Eyert V, Ebbinghaus S G and Kopp T 2006 *Phys. Rev. Lett.* **96** 256401
[13] Eyert V and Ebbinghaus S G 2007 *Prog. Solid State Chem.* **35** 433–9
[14] Wu H *et al* 2006 *Phys. Rev. Lett.* **96** 256402
[15] Riegg S, Günther A, Krug von Nidda H-A, Loidl A, Eremin M V, Reller A and Ebbinghaus S G 2012 *Phys. Rev.* B **86** 115125
[16] Riegg S, Günther A, Krug von Nidda H-A, Eremin M V, Reller A, Loidl A and Ebbinghaus S G 2012 *Eur. Phys. J.* B **85** 413
[17] Guillen M and Bertaut E F 1966 *Bull. Soc. Fr. Ceram.* **72** 57
[18] Petrova M A, Novikova A S and Grebenshchikov R G 2003 *Inorg. Mater.* **39** 509–13
[19] Mumme W G and Wadsley A D 1968 *Acta Crystallogr.* B **24** 1327–33
[20] Tada M, Tomita K, Petrykin V and Kakihana M 2003 *Solid State Ion.* **151** 293–7
[21] Rietveld H M 1969 *J. Appl. Crystallogr.* **2** 65–71
[22] Knapp M, Baehtz C, Ehrenberg H and Fuess H 2004 *J. Synchrotron Radiat.* **11** 328–34
[23] Knapp M, Joco V, Baehtz C, Brecht H H, Berghaeuser A, Ehrenberg H, von Seggern H and Fuess H 2004 *Nucl. Instrum. Methods* A **521** 565–70
[24] Rodriguez-Carvajal J 1993 *Physica* B **192** 55–69
[25] Koepernick K and Eschrig H 1999 *Phys. Rev.* B **59** 1743
[26] Opahle I, Koepernick K and Eschrig H 1999 *Phys. Rev.* B **60** 14035
[27] Khalifah P, Huang Q, Lynn J W, Erwin R W and Cava R J 2000 *Mater. Res. Bull.* **35** 1–7
[28] Shannon R D 1976 *Acta Crystallogr.* A **32** 751–67
[29] Riegg S, Reller A and Ebbinghaus S G 2012 *J. Solid State Chem.* **188** 17–25
[30] Brown I D and Altermatt D 1985 *Acta Crystallogr.* B **41** 244–7
[31] Haynes W M (ed) 2011–2012 *CRC Handbook of Chemistry and Physics* 92nd edn (London: Taylor and Francis)
[32] Krimmel A, Günther A, Kraetschmer W, Dekinger H, Büttgen N, Eyert V, Loidl A, Sheptyakov D V, Scheidt E-W and Scherer W 2009 *Phys. Rev.* B **80** 121101
[33] Bearden J A and Burr A F 1967 *Rev. Mod. Phys.* **39** 125–42
[34] Ebbinghaus S G, Hu Z and Reller A 2001 *J. Solid State Chem.* **156** 194–202
[35] Ressler T 1998 *J. Synchrotron Radiat.* **5** 118–22
[36] Arcon I, Bencan A, Kodre A and Kosec M 2007 *X-Ray Spectrom.* **36** 301–4
[37] Yamamoto T, Mizoguchi T and Tanaka I 2005 *Phys. Rev.* B **71** 245113
[38] Whangbo M-H 1981 *J. Chem. Phys.* **75** 4983